

P2RX₇ sensitizes Mac-1/ICAM-1-dependent leukocyte-endothelial adhesion and promotes neurovascular injury during septic encephalopathy

Huan Wang^{1,2,*}, Ling-Juan Hong^{1,*}, Ji-Yun Huang^{1,*}, Quan Jiang¹, Rong-Rong Tao¹, Chao Tan¹, Nan-Nan Lu¹, Cheng-Kun Wang¹, Muhammad M Ahmed¹, Ying-Mei Lu³, Zhi-Rong Liu⁴, Wei-Xing Shi⁵, En-Yin Lai⁶, Christopher S Wilcox⁷, Feng Han¹

¹Institute of Pharmacology and Toxicology, College of Pharmaceutical Sciences, Zhejiang University, Hangzhou, Zhejiang 310058, China; ²Key Laboratory of Carbohydrate and Lipid Metabolism Research, College of Life Science and Technology, Dalian University, Dalian, Liaoning 116622, China; ³School of Medicine, Zhejiang University City College, Hangzhou, Zhejiang 310015, China; ⁴Department of Neurology, Second Affiliated Hospital of Zhejiang University, School of Medicine, Hangzhou, Zhejiang 310009, China; ⁵Department of Basic Sciences, Loma Linda University Health Schools of Medicine, Pharmacy, and Behavioral Health, Loma Linda, CA 92350, USA; ⁶Department of Physiology, Zhejiang University School of Medicine, Hangzhou, Zhejiang 310058, China; ⁷Hypertension, Kidney, and Vascular Research Center, Georgetown University Medical Center, Washington DC 20007, USA

Septic encephalopathy (SE) is a critical factor determining sepsis mortality. Vascular inflammation is known to be involved in SE, but the molecular events that lead to the development of encephalopathy remain unclear. Using time-lapse *in vivo* two-photon laser scanning microscopy, we provide the first direct evidence that cecal ligation and puncture in septic mice induces microglial trafficking to sites adjacent to leukocyte adhesion on inflamed cerebral microvessels. Our data further demonstrate that septic injury increased the chemokine CXCL1 level in brain endothelial cells by activating endothelial P2RX₇ and eventually enhanced the binding of Mac-1 (CD11b/CD18)-expressing leukocytes to endothelial ICAM-1. In turn, leukocyte adhesion upregulated endothelial CX3CL1, thereby triggering microglia trafficking to the injured site. The sepsis-induced increase in endothelial CX3CL1 was abolished in CD18 hypomorphic mutant mice. Inhibition of the P2RX₇ pathway not only decreased endothelial ICAM-1 expression and leukocyte adhesion but also prevented microglia overactivation, reduced brain injury, and consequently doubled the early survival of septic mice. These results demonstrate the role of the P2RX₇ pathway in linking neurovascular inflammation to brain damage *in vivo* and provide a rationale for targeting endothelial P2RX₇ for neurovascular protection during SE.

Keywords: septic encephalopathy; leukocyte adhesion; P2RX₇; ICAM-1; two-photon imaging; microglia; neurovascular injury

Cell Research (2015) 25:674-690. doi: 10.1038/cr.2015.61; published online 22 May 2015

Introduction

Sepsis is initiated by an uncontrolled infection that

causes a severe systemic inflammatory response and multisystem organ failure [1-3]. Septic encephalopathy (SE) is a serious complication of sepsis that can lead to cerebral atrophy, cognitive impairment, and even mortality [4-6]. Vascular inflammation is known to play a role in the acute brain dysfunction associated with sepsis [1, 7]. MyD88-deficient mice displayed a markedly diminished inflammatory host response in the brain, which was characterized by reductions in the expression of cytokines, chemokines and complement factors [8]. However, ther-

*These three authors contributed equally to this work.

Correspondence: Feng Han^a, Christopher S Wilcox^b

^aTel: +86-571-88208402; Fax: +86-571-88208402

E-mail: changhuahan@zju.edu.cn

^bE-mail: wilcoxch@georgetown.edu

Received 19 October 2014; revised 10 February 2015; accepted 12 March 2015; published online 22 May 2015

apeutic approaches targeting MD2-Toll-like receptor 4 (TLR4) complex have proven ineffective in reducing the mortality of patients with severe sepsis [9], raising the possibility that steps independent of TLR4 signaling in the sepsis inflammatory cascade are more critical for the development of SE and therefore could be better targets for disease intervention. To date, no effective therapies have been identified for the prevention of the neurological dysfunctions associated with SE.

Human SE transitions from systemic inflammation to a diffuse disturbance in the blood-brain barrier (BBB) associated with a period of neurological dysfunction [4]. Several recent studies have suggested roles for vascular factors in SE-related injury of the brain vascular endothelium, changes in BBB permeability and microcirculatory distress [10-12], but the contributions of various cell types, cellular receptors and signaling events remain unclear [13-15]. For example, although leukocyte adhesion to activated endothelial cells has been identified as an early event in sepsis-related central nervous system dysfunction [16], the triggers of this event and the mechanism by which leukocyte adhesion may lead to the development of encephalopathy remain uncertain. Microglia act as unique primary immune cells in the brain and function as the main defense against brain injury [17, 18]. Microglial activation increases the production of reactive oxygen species and contributes to the progression of brain damage during SE [19]. Therefore, the goal of this study is to determine the potential link between leukocyte adhesion and microglia overactivation during sepsis.

The temporary systemic inflammation caused by endotoxemia in humans cannot directly trigger the development of SE [20]. Recently, P2RX₇ activation was shown to amplify lipopolysaccharide (LPS)-induced hyporeactivity in the endothelium-intact mouse aorta [21]. Because brain endothelial activation during sepsis significantly impacts microcirculation and BBB integrity [13-15], we hypothesized that P2RX₇ plays a critical role in sepsis-induced neurovascular damage. P2RX₇ is an ATP-gated purinoceptor channel that mediates Ca²⁺ influx and subsequent downstream intracellular signaling events [22, 23]. P2RX₇ regulates the immune responses and disease pathogenesis by activating the NLRP3-inflammasome in macrophages and secretion of the proinflammatory cytokine interleukin-1 β (IL-1 β) [24].

Using *in vivo* two-photon laser scanning microscopy (TPLSM) combined with genetic deletion and pharmacological blockade, this study is the first to demonstrate that endothelial P2RX₇ activation is a key step in initiating both leukocyte adhesion and microglia recruitment during SE. Here, we report a novel function for endothe-

lial P2RX₇ in Mac-1/ICAM-1-mediated attachment of sensitized leukocytes to the brain microvascular endothelium and in subsequent endothelial CX3CL1 elevation during SE. More importantly, we show that inhibition of the brain endothelial P2RX₇ signaling pathway significantly reduced the mortality of septic mice. Thus, the P2RX₇ signaling pathway could be a novel target for the treatment of SE.

Results

Two-photon imaging of leukocyte recruitment and motility in brain vessels after cecal ligation and puncture

Cerebral lesions in humans with sepsis are found in the cortical and subcortical region [25]. In this study, video images of brain vessels were used to study leukocyte-endothelial cell adhesion in single cerebral blood vessels in living mice (Supplementary information, Figure S1). A rapid acquisition rate (30 frames/s) was used to capture sequential images of rhodamine 6G-labeled leukocytes as they streaked rapidly through the microcirculation in mice (Figure 1A and Supplementary information, Figure S2).

Rolling, loosely adherent and arrested or firmly adherent leukocytes were quantified at 4 h post-cecal ligation and puncture (CLP) using time-lapse imaging (Supplementary information, Figure S2 and Movie S1). A firmly adherent cell was defined as a rhodamine 6G-positive single cell that remained stationary along the inner surface of the vessel wall for at least 1 min. In contrast, leukocytes from sham-operated controls exhibited rolling or little adherence to the cortical microvasculature (Supplementary information, Figure S2). The number of adherent leukocytes (loosely adherent/arrested or firmly adherent) at 4 h post-CLP was increased by $458 \pm 102/\text{mm}^2$ compared to that in the sham mice ($26 \pm 10/\text{mm}^2$; Figure 1A and 1B), and remained elevated for at least 16 h (Figure 1A, 1B and Supplementary information, Movie S2). Leukocyte adhesion was matched by a significant reduction in the rolling velocity in the brain microvessels of CLP mice (Figure 1C and 1D). Therefore, endothelial activation and leukocyte adhesion may form one of the earliest stages in the progression of SE. These results provide the first *in vivo* evidence for leukocyte adhesion following CLP.

Interplay between leukocyte adhesion and microglia activation following CLP

The early innate immune response following sepsis [26] was captured by TPLSM imaging *in vivo* to determine the dynamic changes in leukocyte-endothelial adhesion in *Cx3cr1*^{GFP/+} mice. *Cx3cr1*^{GFP/+} mice are use-

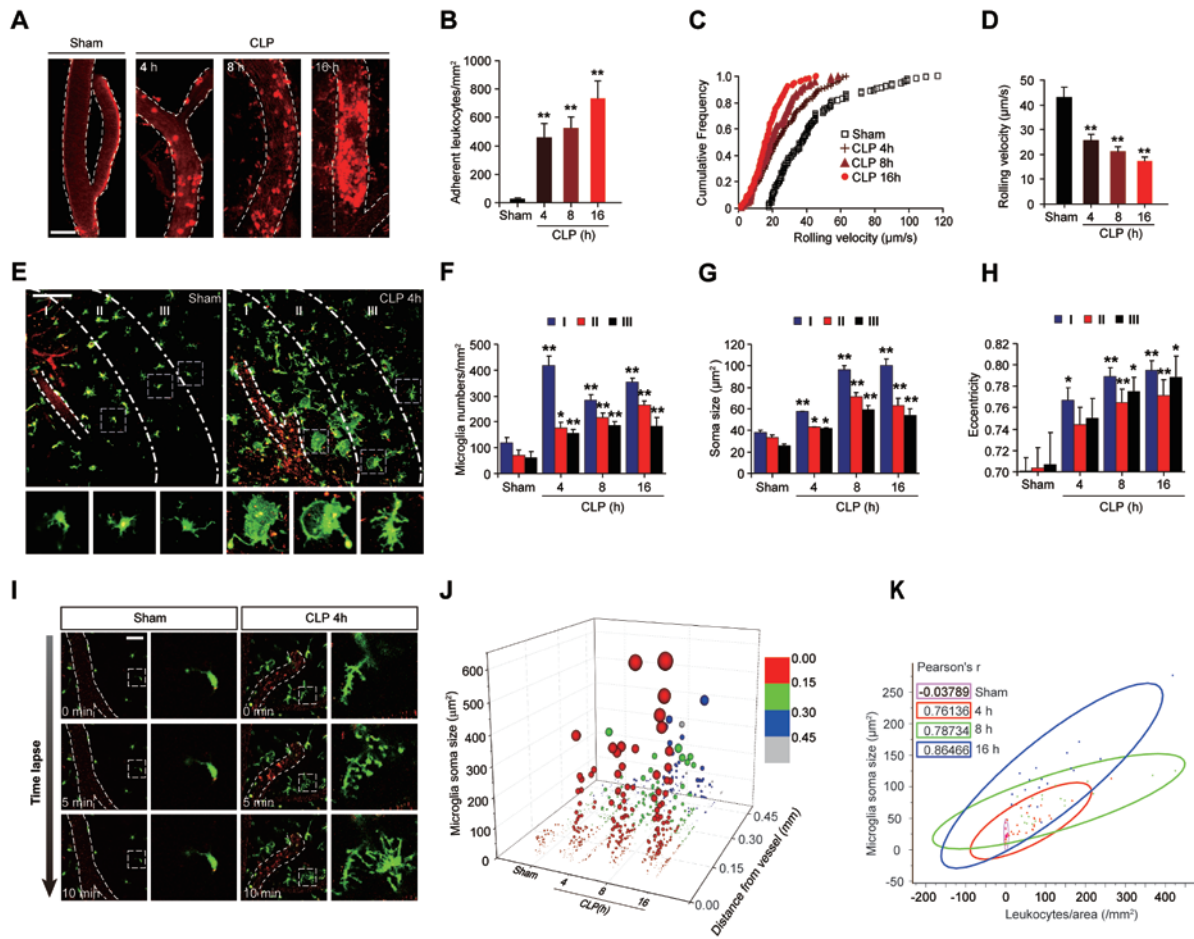


Figure 1 *In vivo* two-photon imaging to assess temporal changes in leukocyte adhesion and the graded morphological changes of microglial cells in living mice following CLP. For two-photon imaging, cortical brain vessels (20–40 μm in diameter and 100–150 μm in depth below the cortical surface) were selected for imaging. **(A)** Rhodamine 6G-labeled leukocytes were visualized for adhesion in brain vasculature at 4, 8 and 16 h after CLP. The first panel shows baseline adhesion. Other panels represent images of leukocyte marginalization and adhesion in brain vessels (white dashed lines). Scale bar, 30 μm . **(B)** Quantitative measurements of firmly adhering leukocytes at the indicated time points after CLP. Adherent leukocytes from at least three fields of view per animal were counted as the number of cells per mm^2 of vascular surface area. The results are shown as means \pm SEM ($n = 6$). $**P < 0.01$ versus sham. **(C)** The Scatter plots show that the cumulative frequency of rolling velocities of leukocytes in the indicated groups. **(D)** The histogram shows a significant reduction in rolling velocities in CLP mice compared with sham mice. Rolling velocities of 115 cells per group (means \pm SEM, $n = 4$ mice) were measured. $**P < 0.01$ versus sham. **(E)** *Cx3cr1*^{GFP/+} mice were used to visualize the kinetics of microglia and activated microglia 4 h after CLP. The morphological changes of microglial cells were consistently observed at regions I, II and III with regular $\sim 150 \mu\text{m}$ intervals toward the center of brain vessels by using intravital TPLSM. Scale bar, 100 μm . **(F)** The number of GFP⁺ microglia was significantly increased 4 h following CLP. **(G, H)** Changes in microglial soma size (μm^2) and eccentricity were measured in *Cx3cr1*^{GFP/+} mice at the indicated time points after CLP. Quantification of microglial eccentricity reflects the uniform central to peripheral distribution of microglia cells measured *in vivo*. Data are expressed as means \pm SEM ($n = 6$ mice). $*P < 0.05$; $**P < 0.01$ versus sham. **(I)** Time-lapse series showing progressive extension of microglia processes toward local brain vessels. Microglial behavior was recorded by intravital TPLSM 4 h after CLP. Images are individual frames from a continuous time-lapse movie and show progressive morphological changes occurring over a recording period of 10 min. Times are given in minutes. Unlike behavior of cells in sham mice (left panel), images of CLP mice (right panel) show that microglia extend processes (green) toward local brain vessels (white dashed lines) over time. The insets show zoomed morphological changes of microglia endfeet (green) next to vessels. Scale bar, 100 μm . **(J)** Sepsis-induced activation and redistribution of microglia cells were related to the distance from the inflamed vessels. Mean values of microglia soma size (μm^2) in regions I, II and III were measured at the indicated time points after CLP. **(K)** Scatterplots of firmly adherent leukocytes (x -axis) and corresponding microglial soma size (y -axis) in sham, 4, 8 and 16 h after CLP. Linear correlation analysis indicates that leukocyte-endothelial cell adhesion (per mm^2) is closely associated with changes in soma size of microglia (μm^2) during CLP. The ellipse stands for 95% confidence level.

ful for visualizing microglia due to the expression of the enhanced green fluorescent protein (GFP) $\leq 150 \mu\text{m}$ beneath the pial surface [27, 28]. There was a consistent gradient of morphological changes in microglial cells radiating out from the distal border of brain vessels. Slices of $\sim 150 \mu\text{m}$ were used to define regions I, II and III from the center of a region of firmly adherent leukocyte-endothelial cell interaction inside the vessels (Figure 1E). The number of microglial cells with amoeboid morphology surrounding the inflamed brain vessels was increased in the CLP mice (region I > region II > region III, Figure 1E). A quantitative metric used to analyze microglia activation *in vivo* [29] demonstrated that microglia number (Figure 1F), soma size (Figure 1G) and eccentricity (Figure 1H) all increased circumferentially around the inflamed vessels at 4 h post-CLP and remained elevated for at least 16 h. These observations led us to examine the correlation between leukocyte-endothelial adhesion and morphological changes in microglia following CLP.

Changes in the morphology and motility (assessed from outgrowth processes) of activated microglia [27] were obvious in mice at 4 h post-CLP (10 min recording, Figure 1I, right panel), but were absent in the sham-operated mice. The diverging growth cones began to fan out from the points of vascular inflammation at 4 h post-CLP (10 min recording, Figure 1I, right panel, and Supplementary information, Movie S3). Moreover, the activation and redistribution of microglial cells were dependent on the distance from the inflamed vessels in the CLP mice (Figure 1J). Linear correlation analysis demonstrated that leukocyte-endothelial cell adhesion during CLP was closely associated with changes in the microglial cell area (Figure 1K). To further confirm the correlation between leukocyte-endothelial adhesion and microglial activation, we depleted leukocytes using an anti-granulocyte receptor-1 (Gr-1) monoclonal antibody (mAb, RB6-8C5). Treatment with RB6-8C5 significantly suppressed microglial activation (Supplementary information, Figure S3).

Sepsis increases brain endothelial chemokine expression

The CXCL1 family of cytokines promotes granulocyte adhesion to brain capillaries during encephalomyelitis [30]. mRNA analysis of *CXCL1*, *CXCL5*, *CXCL10*, *CX3CL1*, *CCL2* and *CCL3* in brain microvessel extracts at 4 h post-CLP, showed significant increases in *CXCL1* and *CX3CL1* (Figure 2). Consistently, the endothelial localization of *CXCL1* and *CX3CL1* in brain microvessels was also observed 4 h post-CLP (Supplementary information, Figure S4A and S4B). We detected elevated blood levels of *CXCL1* but not *CX3CL1* 4 h post-CLP (Supplementary information, Figure S4C). The increased

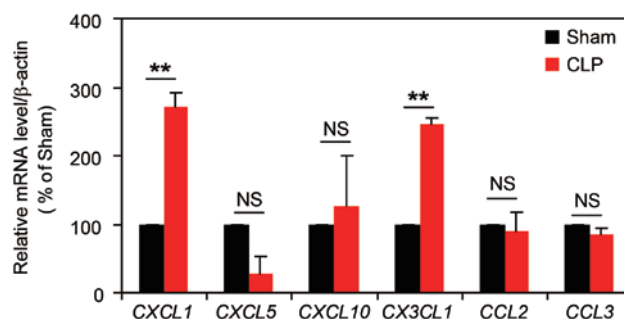


Figure 2 Sepsis increases brain endothelial chemokine expression. The chemokine *CXCL1*, *CXCL5*, *CXCL10*, *CX3CL1*, *CCL2* and *CCL3* mRNA levels from mouse brain endothelial cells were measured. The chemokine mRNAs were determined by real-time PCR analysis 4 h after CLP. Data are presented as a percentage change (%) compared to the sham control (means \pm SEM, $n = 4$). ** $P < 0.01$. NS, not significant.

blood *CXCL1* level in SE may be caused by the induction of proteolytic cleavage of chemokines from endothelial cells [31].

CXCL1 promotes leukocyte adhesion via $\beta 2$ integrin/ICAM-1 signaling

The $\beta 2$ integrin is crucial for the adhesion of circulating leukocytes to endothelial cells via binding to ICAM-1 [32]. Our data demonstrate that Mac-1/CR3 (CD11b/CD18) but not LFA-1 (CD11a/CD18) plays a role in leukocyte adhesion to the vascular endothelium during sepsis (Figure 3A). Endothelial expression of ICAM-1 was activated consistently within 4 h post-CLP (Figure 3B).

To gain further insight into the roles of the $\beta 2$ integrin/ICAM-1 pathway in sepsis, a *CXCL1*-neutralizing antibody was used in the CLP mouse model. As shown in Figure 3C, *CXCL1*-neutralizing antibody (50 μg) treatment significantly decreased the adhesion of rhodamine 6G-labeled leukocytes to brain vessels by 76.1% ($P < 0.01$) at 4 h post-CLP. Moreover, decreased levels of endothelial ICAM-1 were observed in CLP mice after *CXCL1*-neutralizing antibody treatment (Figure 3D). Interestingly, *CXCL1* neutralization also decreased the levels of *CXCL1* and *CX3CL1* mRNA induced by CLP (Figure 3E). In contrast, *CCL2*- or *CXCL7*-neutralizing antibody treatment did not reduce either leukocyte adhesion (Supplementary information, Figure S5A) or endothelial ICAM-1 expression in CLP mice (Supplementary information, Figure S5B).

CX3CL1 recruits microglia

CX3CL1-*CX3CR1* signaling has been implicated in

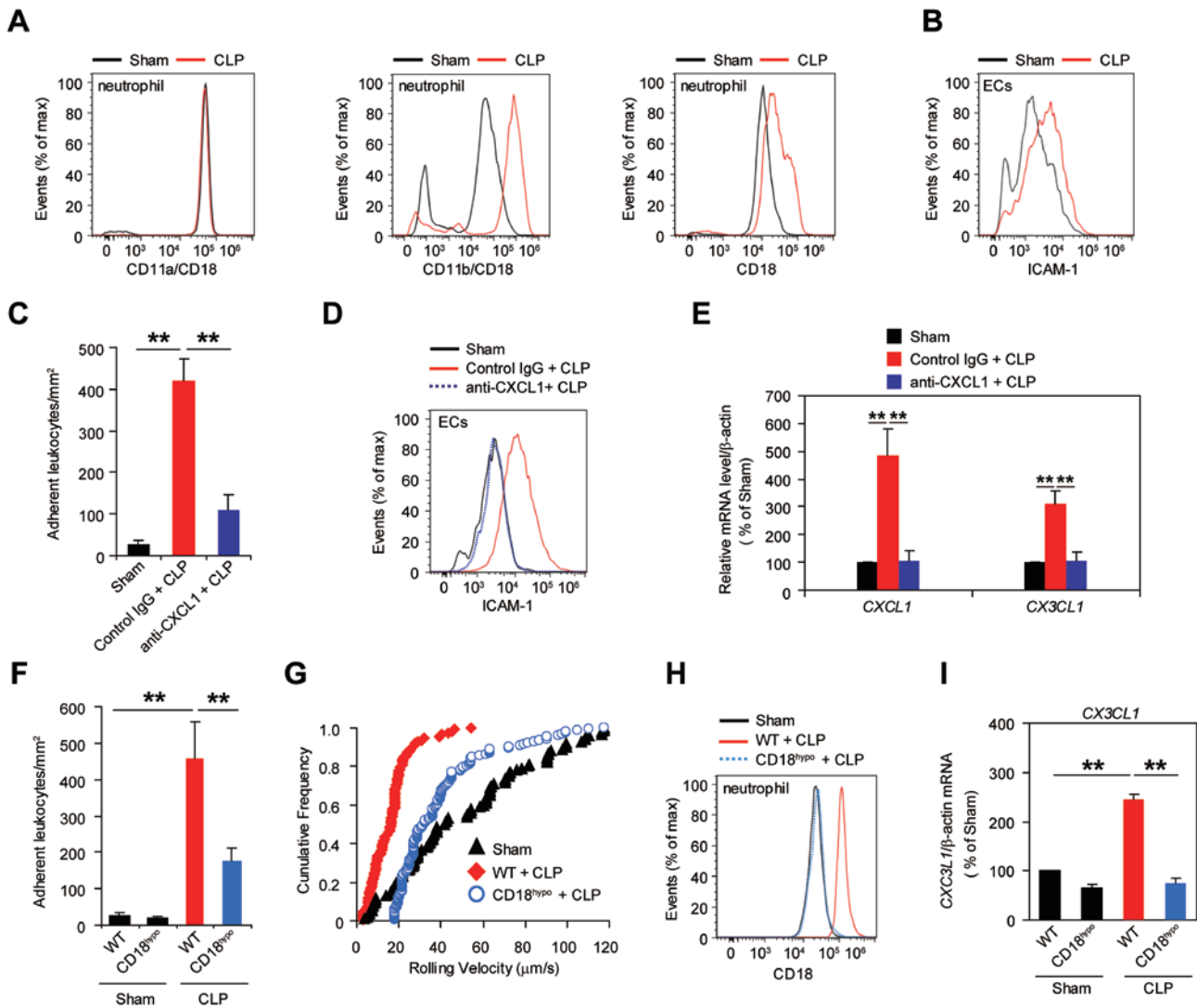


Figure 3 CXCL1 promotes leukocyte adhesion via β 2 integrin/ICAM-1 signaling. **(A)** Flow cytometry analysis of the surface expression of CD11a/CD18, CD11b/CD18 and CD18 on leukocytes (labeled by Ly6G staining) from peripheral blood of Sham mice and CLP (4 h) mice. **(B)** Surface staining of ICAM-1 on vascular endothelial cells in Sham and CLP mice. Data are representative of three independent experiments with three mice per group. **(C, D)** CXCL1-neutralizing antibody treatment significantly inhibited leukocytes adhesion **(C)** and endothelial ICAM-1 elevation **(D)** in CLP mice. IgG treatment (Control IgG) serves as control. The results are shown as means \pm SEM ($n = 4$). $**P < 0.01$. Flow cytometry data are representative of three independent experiments with four mice per group. **(E)** CLP-induced *CXCL1* and *CX3CL1* mRNA elevation in brain vessels were abrogated after CXCL1-neutralizing antibody treatment. Data are expressed as means \pm SEM ($n = 4$). $**P < 0.01$. **(F, G)** CLP induced leukocyte-endothelial cell adhesion **(F)** and the cumulative frequency of rolling velocities of leukocytes **(G)** was reduced in CD18 hypomorphic mutant (*CD18^{hypo}*) mice. Two-photon imaging results are shown as means \pm SEM ($n = 4$). $**P < 0.01$. **(H)** CLP-induced leukocyte β 2 integrin elevation was abrogated in *CD18^{hypo}* mice. Flow cytometry data are representative of three independent experiments with four mice per group. **(I)** The *CX3CL1* mRNA level was reduced in *CD18^{hypo}* mice 4 h after CLP. Data are expressed as means \pm SEM ($n = 4$). $**P < 0.01$.

the cell-to-cell communications underlying microglial chemotaxis and microglial activation [33, 34]. Consistent with this notion, the mRNA levels of *CX3CL1* were increased in brain microvessel extracts after CLP (Figure

2). Also, exogenous recombinant CX3CL1 increased the migration of BV-2 microglia in cell culture but CXCL1 did not (Supplementary information, Figure S6). Importantly, CX3CL1-neutralizing antibody treatment signifi-

cantly decreased microglial activation in the CLP mice (Supplementary information, Figure S7A-S7C). To determine whether CX3CL1 is generally required for CXCL1 elevation, endothelial *CXCL1* mRNA was examined after CLP. We found that CX3CL1 treatment had no effect on endothelial *CXCL1* mRNA or ICAM levels (Supplementary information, Figure S7D and S7E).

CLP-induced endothelial CX3CL1 expression also depends on β 2 integrin/ICAM-1 signaling

As described above, CXCL1 promoted leukocyte adhesion via β 2 integrin/ICAM-1 signaling. CD18 hypomorphic mutant mice were used (resulting in very low expression of the β 2 integrin protein) to test whether the β 2 integrin/ICAM-1 pathway is also involved in CLP-induced CX3CL1 expression. The mutant mice showed greatly reduced leukocyte adhesion following CLP compared to the WT mice ($P < 0.05$; Figure 3F and 3G). The increase in the expression of β 2 integrin (CD18) on leukocytes upon CLP was abrogated in the mutant mice (Figure 3H). In parallel to these changes, the CLP-induced increase in *CX3CL1* mRNA was also eliminated (Figure 3I). These results support the hypothesis that the β 2 integrin and its endothelial ligand are involved not only in leukocyte adhesion to the endothelium but also in the CX3CL1-dependent microglial activation induced by CLP.

Increased P2RX₇ signaling in cerebral microvessels post-CLP

A panel of markers was investigated post-CLP to identify the septic inflammatory stimuli that initiate leu-

kocyte adhesion and microglial activation. Dual labeling of P2RX₇ and ICAM-1 demonstrated their concurrent activation in brain endothelial cells (Figure 4A and 4B). Immunoreactive P2RX₇ but not P2RX₄ was increased in microvessel lysates at 4 h post-CLP; this finding was consistent with the elevated endothelial NLRP3 expression (Figure 4C and 4D). Thus, P2RX₇ is likely to be activated by the massive release of ATP during septic shock [35-37]. Next, we examined the biological variation in endothelial P2RX₇ expression among different tissues. RT-PCR analysis showed a higher expression level of P2RX₇ mRNA in brain vessels than in the aortic and kidney endothelia of mice (Supplementary information, Figure S8A). Additionally, P2RX₇ expression was not significantly different in aortic artery and kidney vessels until at least 4 h post-CLP compared to that in the sham mice (Supplementary information, Figure S8B).

P2RX₇ regulates immune responses and disease pathogenesis via activation of the NLRP3-inflammasome and secretion of the proinflammatory cytokine IL-1 β [24]. The processing of pro-IL-1 β and activation of caspase-1 (p10; a component of the NLRP3-inflammasome) were increased in the cortex early after CLP and remained elevated for at least 16 h concurrent with increased MMP-9 expression, indicating neurovascular damage (Supplementary information, Figure S9).

P2RX₇ knockdown ameliorates leukocyte-endothelial cell adhesion in septic mice

The requirement of P2RX₇ signaling for leukocyte-endothelial cell adhesion was investigated using P2RX₇-specific shRNA transfection in septic mice. In-

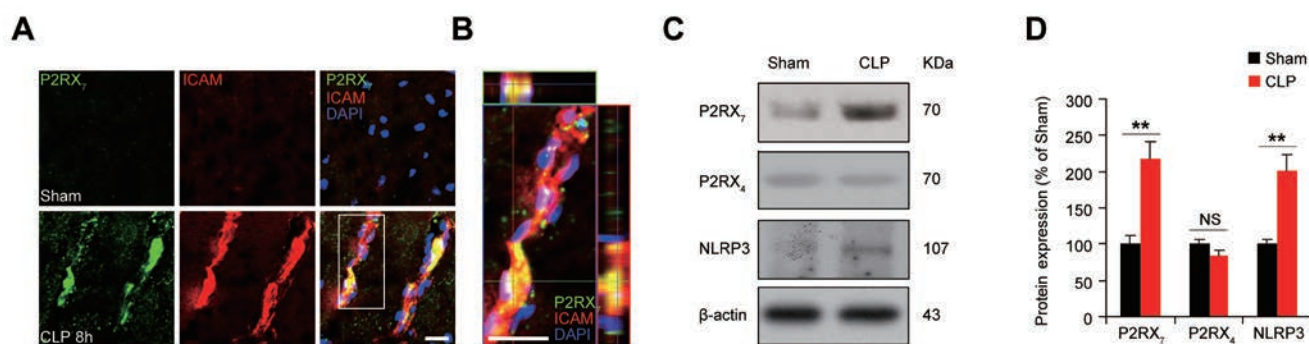


Figure 4 Increased P2RX₇ signaling in cerebral microvessel after CLP. **(A)** Representative images of P2RX₇ (green) and ICAM-1 (red) in brain cortex after CLP. Double labeling revealed co-localization of P2RX₇ and ICAM-1 in brain vessels 4 h after CLP. Scale bar, 20 μ m. DAPI counterstaining indicates cell nuclei (blue). **(B)** Enlarged view of boxed area in **A** showing colocalization of P2RX₇ and ICAM-1 after CLP. Scale bar, 20 μ m. **(C)** Representative immunoblots showing P2RX₇ and NLRP3 expression in microvessel extracts of sham-operated and CLP mice (mean \pm SEM, $n = 5$). **(D)** Quantitative analysis of protein levels in **C** was performed by densitometry. Data are expressed as densitometry ratio of control. The data are expressed as percentages of values obtained from sham animals (mean \pm SEM, $n = 5$). ** $P < 0.01$. NS, not significant.

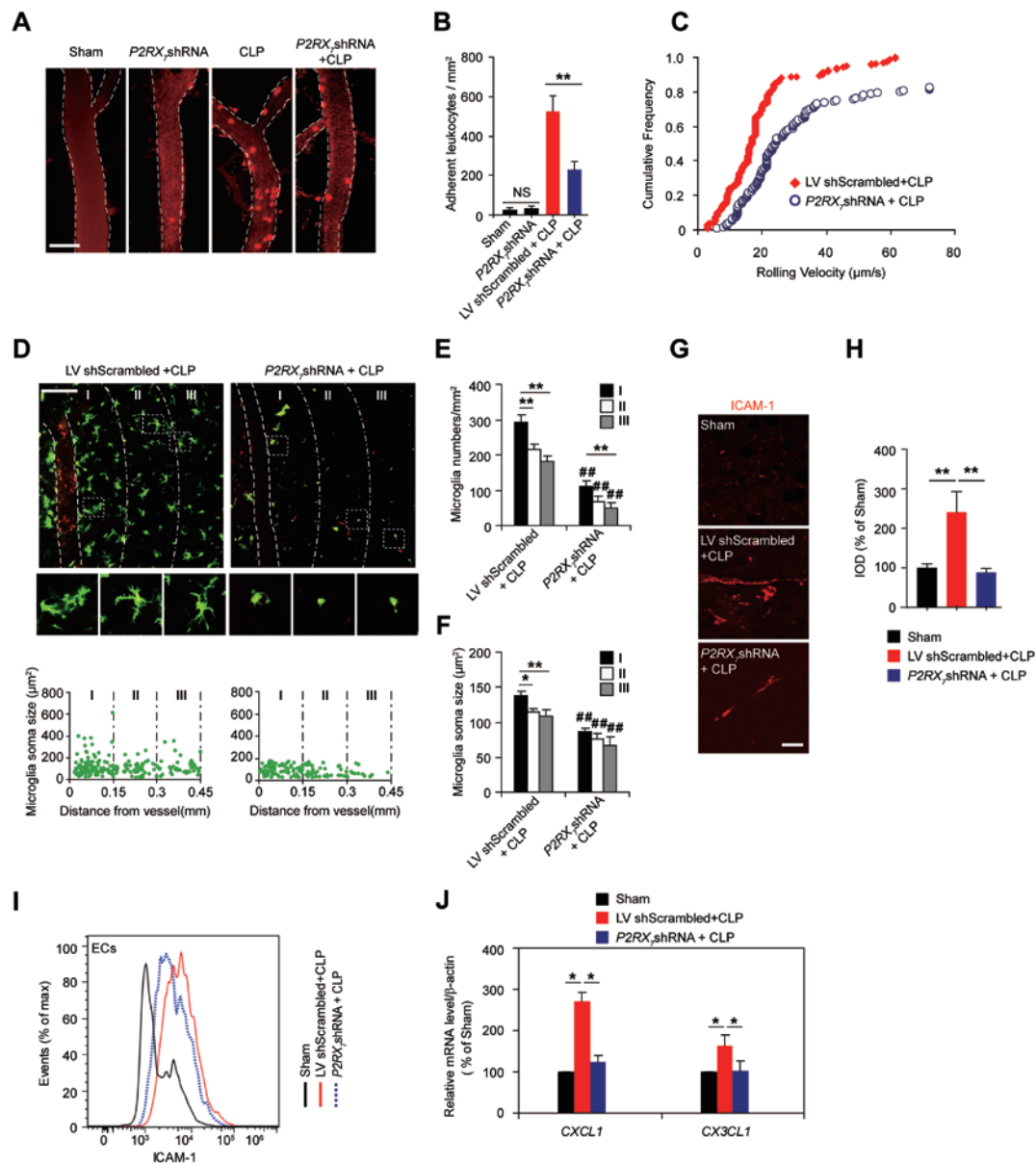


Figure 5 P2RX₇ knockdown ameliorates leukocyte-endothelial cell adhesion in septic mice. **(A)** Representative images from TPLSM analysis of leukocyte adhesion to brain vessels 4 h after CLP. The mice were treated intracerebroventricularly with either a scrambled shRNA (LV shScrambled) or P2RX₇ shRNA two weeks before CLP. Scale bar, 30 µm. **(B)** Quantitative analysis of adherent leukocytes in **A**. Results are shown as means ± SEM (n = 4). **P < 0.01. NS, not significant. **(C)** In lenti-P2RX₇ shRNA group, the cumulative frequency of rolling velocities of leukocytes showed a significant reduction compared with lenti-shScramble-treated group after CLP. Rolling velocities of 138 cells per group (n = 4 mice) were measured. **(D)** The representative changes of morphological parameters of microglial cells by lenti-P2RX₇ shRNA transfection were observed at regions I, II and III by using intravital TPLSM. Scale bar, 100 µm (upper panel). Microglia in regions I, II and III were mapped at 4 h after CLP (lower panel). **(E, F)** Microglia numbers **(E)** and mean values of microglia soma size **(F)** in regions I, II and III were measured after CLP. Data are expressed as means ± SEM (n = 6). *P < 0.05, **P < 0.01 versus region I; ###P < 0.01 versus LV shScramble + CLP mice. **(G)** The immunohistochemical staining for ICAM (red) in sham, lenti-shScramble and P2RX₇ shRNA group at 8 h after CLP. Scale bar, 20 µm. **(H)** Quantification of ICAM fluorescent signals in brain microvessels from **G** (mean ± SEM, n = 4 mice). **P < 0.01. **(I)** Effect of lenti-P2RX₇ shRNA transfection on endothelial ICAM-1 expression in CLP mice. Flow cytometry analysis shows the surface staining of ICAM-1 in the indicated groups. Data are representative of three independent experiments with four mice per group. **(J)** P2RX₇ knockdown decreased CXCL1 and CX3CL1 mRNA levels in brain microvasculature of CLP mice. The upregulation of chemokine CXCL1 and CX3CL1 mRNA level was inhibited after P2RX₇ shRNA treatment in CLP mice. Data are expressed as means ± SEM (n = 4). *P < 0.05.

tracerebroventricular injection of a lentiviral vector encoding a $P2RX_7$ -specific shRNA significantly suppressed the adhesion of rhodamine 6G-labeled leukocytes to the brain vessels at 4 h post-CLP by 56% versus the control lenti-shScramble-treated mice ($P < 0.01$, Figure 5A and 5B). The delivery of $P2RX_7$ shRNA to sham mice had no effect (Figure 5A and 5B). Blocking $P2RX_7$ signaling by lentivirus- $P2RX_7$ shRNA transfection increased the leukocyte rolling velocity in mice with CLP (Figure 5C) and reduced the activation of microglia in $Cx3cr1^{GFP/+}$ mice (Figure 5D-5F and Supplementary information, Figure S10). The inhibitory effect of $P2RX_7$ shRNA on ICAM-1 level was visualized by immunostaining of the microvessels (Figure 5G and 5H) and flow cytometry analysis (Figure 5I). Moreover, $CXCL1$ and $CX3CL1$ mRNA levels in brain microvessel extracts were significantly decreased by lentivirus- $P2RX_7$ shRNA transfection (Figure 5J). These results suggest that endothelial $P2RX_7$ is involved in the initiation of both leukocyte adhesion and

microglial activation.

Pharmacological blockade of $P2RX_7$ reduces adhesion molecule expression in mice with CLP

To confirm that $P2RX_7$ activation is required for Mac-1/ICAM-1-dependent leukocyte adhesion, we used the $P2RX_7$ antagonist A438079. Blockade of $P2RX_7$ by A438079 reduced the number of adherent leukocytes and increased their rolling velocities (Figure 6A and 6B). Flow cytometry showed that A438079 reduced the expression of ICAM-1, but had no effect on the expression of VCAM-1 (Figure 6C and 6D). These results are consistent with the fact that ICAM-1 initiates leukocyte adhesion by interacting with its specific counter-receptor β_2 integrins (LFA-1 and Mac-1) on leukocytes, whereas VCAM-1 binds to very late antigen 4 on monocytes, which do not cluster until the adhesion sites mature [38]. These results, combined with those obtained with $P2RX_7$ shRNA, further support the hypothesis that $P2RX_7$ ac-

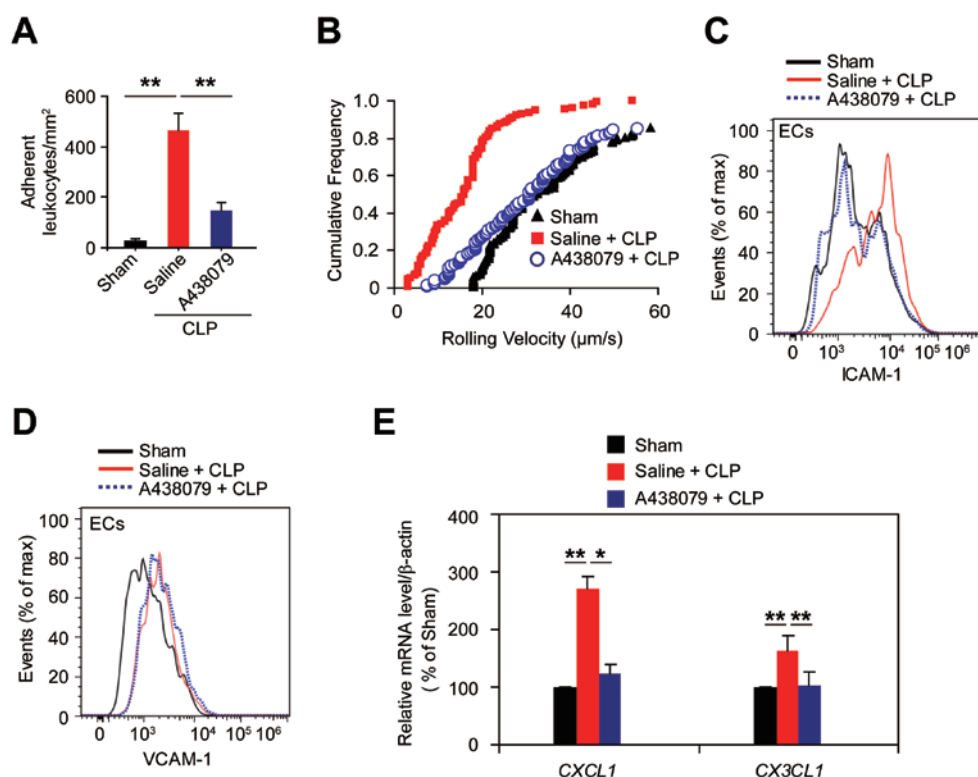


Figure 6 $P2RX_7$ inhibition reduces the adhesion molecules in brain microvasculature of CLP mice. **(A)** Adherent leukocytes were decreased in A438079-treated mice versus saline-treated mice 4 h after CLP. The results are shown as the means \pm SEM ($n = 4$). $**P < 0.01$. **(B)** The Scatter plots show the cumulative frequency of rolling velocities of leukocytes in each treatment conditions. **(C, D)** Changes of brain endothelial ICAM-1 and VCAM-1 levels from CLP mice with or without A438079 treatment. Flow cytometry analysis shows the surface staining of ICAM-1 and VCAM-1 in the indicated groups. Data are representative of three independent experiments with four mice per group. **(E)** The chemokine $CXCL1$ and $CX3CL1$ mRNA levels were decreased in CLP mice after A438079 treatment. Data are expressed as means \pm SEM ($n = 4$). $*P < 0.05$, $**P < 0.01$.

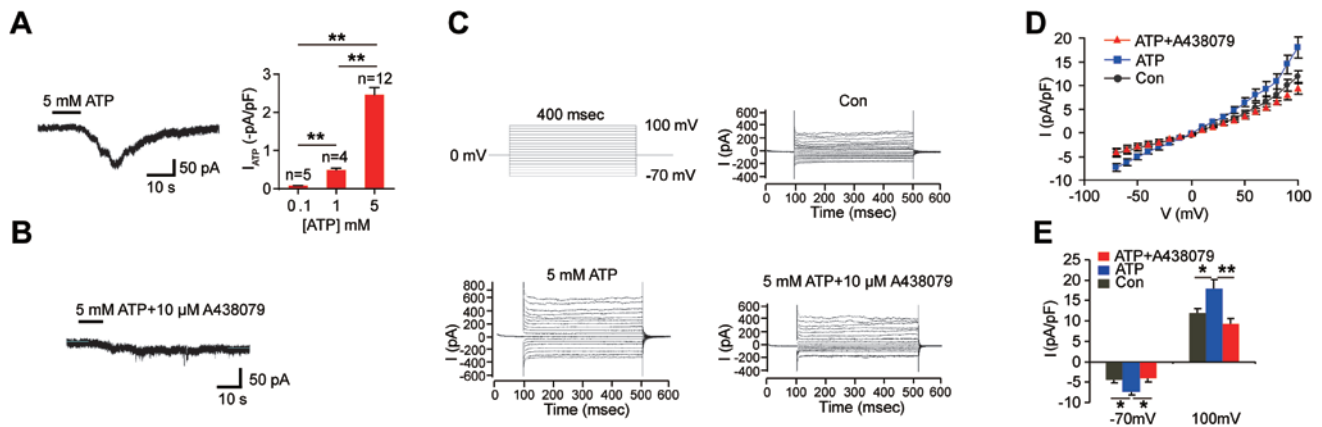


Figure 7 Effect of pharmacological inhibition on brain endothelial P2RX₇ cation channel currents. **(A)** Whole-cell patch clamp recordings from HBMEC at the holding potential of -70 mV. Histogram summarizes the mean peak currents normalized to membrane capacitance detected at the given ATP concentrations. Data are expressed as means \pm SEM. ****** $P < 0.01$. **(B)** Pharmacological evidence for the localization of P2RX₇ receptors in HBMEC. 5 mM ATP was applied in the presence of P2RX₇ antagonist (A438079, 10 μ M). **(C)** Electrophysiological features of P2RX₇ channel in brain endothelial cells. Increased cation channel currents by ATP application were blocked with pretreatment of A438079. **(D)** Effect of P2RX₇ inhibition on ATP-induced activation of nonselective cation channel currents. The currents were normalized to capacitance to obtain current density (pA/pF). **(E)** Quantification data for **D**. A438079 decreased ATP-induced inward currents and outward currents ($n = 11$; $*P < 0.05$, $**P < 0.01$).

tivation initiates leukocyte-endothelial cell adhesion by increasing ICAM-1 expression. A438079 application also inhibited the endothelial expression of *CXCL1* and *CX3CL1* induced by CLP (Figure 6E).

The P2RX₇ receptor is a nonselective cation channel that is involved in many pathophysiological processes [22, 23]. To study its functional expression on endothelial cells and to confirm that A438079 blocks P2RX₇ receptor-mediated effects, whole-cell patch clamp recordings were performed in human brain microvascular endothelial cell (HBMEC). At the holding potential of -70 mV, a brief application (10 s) of ATP elicited a dose-dependent inward current with a mean density of 2.46 ± 0.17 pA/pF (Figure 7A). Co-application of A438079 (10 μ M) reversibly inhibited the currents induced by 5 mM ATP by 82% (Figure 7B and 7C). ATP (5 mM) application increased the whole-cell slope conductance and increased both the inward and outward currents (Figure 7C). The outward rectifying currents were increased from 11.86 ± 1.25 pA/pF to 17.91 ± 2.19 pA/pF ($P < 0.05$ versus control), and the inward currents were increased from 4.38 ± 0.81 pA/pF to 7.31 ± 0.85 pA/pF ($P < 0.05$ versus control, Figure 7D and 7E). A438079 blocked all of the effects induced by ATP (Figure 7D and 7E). P2RX₇ activation is unusual in that it elicits the influx of large molecular weight cations, such as the fluorescent dye ethidium (Et⁺) [39]. Co-application of 10 μ M A438079 also abolished ATP (1 mM)-induced Et⁺ influx into HBMEC (Supplemen-

tary information, Figure S11). These results confirm the expression of P2RX₇ on brain endothelial cells, where it functions as an ion channel and mediates cation channel conductance.

IL-1 β mediates the effect of P2RX₇

P2RX₇ activation has been shown to increase IL-1 β release in a P2RX₇ cation current-sensitive fashion [40]. Activation of the P2RX₇ receptor in microvessels has been shown to induce secretion of IL-1 β [41]. To test whether the effect of P2RX₇ is in part mediated through IL-1 β , we treated mice with an anti-IL-1 β mAb. The treatment significantly suppressed leukocyte adhesion to brain vessels (Figure 8A) and increased the rolling velocities of leukocytes (Figure 8B) at 4 h post-CLP. Endothelial ICAM-1 (Figure 8C) and VCAM-1 (Figure 8D) expression were increased 4 h post-CLP. Anti-IL-1 β treatment inhibited the expression of ICAM-1, but not the expression of VCAM-1, induced by CLP (Figure 8C and 8D). Anti-IL-1 β also abolished the CLP-induced increase in the *CXCL1* and *CX3CL1* mRNA levels (Figure 8E).

Neurovascular injury after CLP is dependent on the activation of P2RX₇ signaling

Although leukocyte-endothelial cell adhesion was well-developed in the cerebral vessels of WT mice post-CLP ($524 \pm 88/\text{mm}^2$), it was sparse in the vessels of

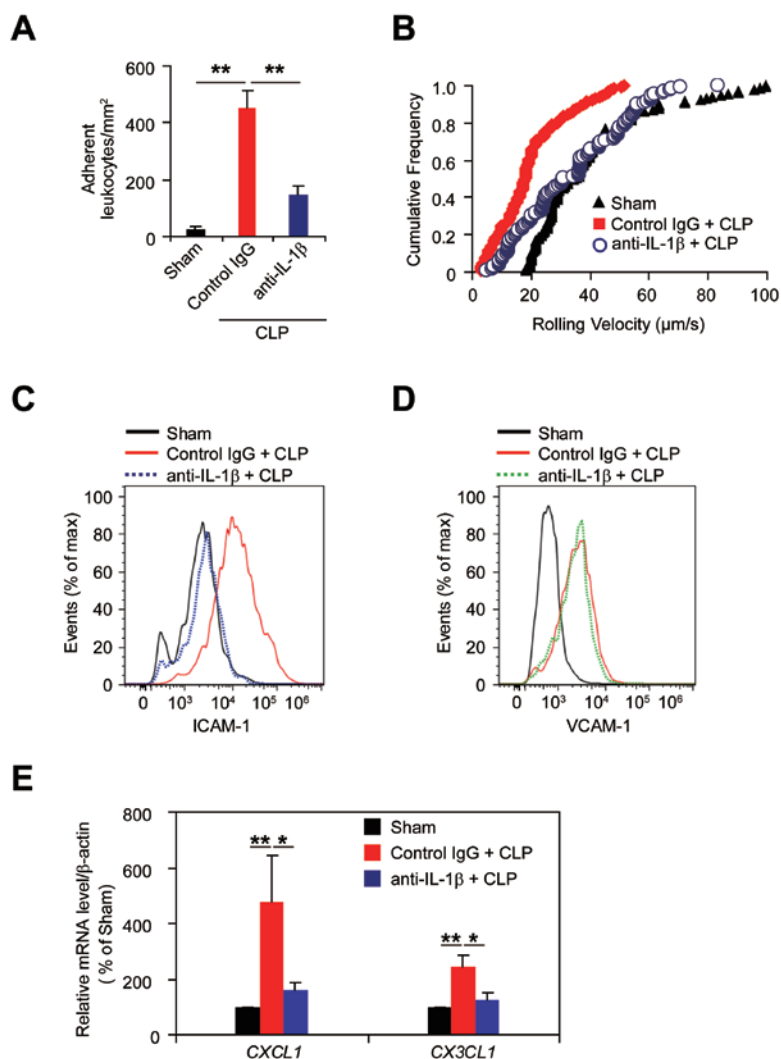


Figure 8 Effect of IL-1 β neutralization on expression of adhesion molecules in CLP mice. **(A)** Adherent leukocytes were decreased in IL-1 β -neutralizing antibody-treated mice versus IgG-treated mice (Control IgG) 4 h after CLP. The results are shown as means \pm SEM ($n = 4$). $**P < 0.01$. **(B)** IL-1 β -neutralizing antibody treatment decreased the cumulative frequency of rolling velocities of leukocytes after CLP. Rolling velocities of 128 cells per group ($n = 4$) were measured. **(C, D)** The brain endothelial cells were isolated from sham and CLP mice and labeled with ICAM-1 and VCAM-1, respectively. IL-1 β -neutralizing antibody treatment inhibits the expression of ICAM-1 4 h after CLP. Data are representative of three independent experiments with three mice per group. **(E)** IL-1 β -neutralizing antibody treatment reduced chemokine *CXCL1* and *CX3CL1* mRNA levels in brain endothelial cells of CLP mice. Data are expressed as means \pm SEM ($n = 4$). $*P < 0.05$; $**P < 0.01$.

P2RX₇^{-/-} mice ($204 \pm 66/\text{mm}^2$; $P < 0.01$ versus WT mice; Figure 9A and 9B). The brains of *P2RX₇^{-/-}* mice at 8 h post-CLP showed evidence of better BBB preservation, with reduced elevation in the expression of the breakdown product of ZO-1 and spectrin, reduced upregulation of caspase-1 (p10), IL-1 β (p17) and MMP-9, but, unexpectedly, unchanged expression of the Fas-associated death domain (FADD; Figure 9C and 9D; Supplementary information, Figure S12). These findings suggest that Fas ligands and Fas signaling are not involved in the brain's

responses to sepsis. Double labeling with Fluoro-Jade B (FJB) and antibodies to neuron-specific nuclear antigen demonstrated increased numbers of FJB-positive cells in WT mice following CLP, whereas fewer FJB-positive cells were present in the *P2RX₇^{-/-}* mice (Figure 9E). Kaplan–Meier survival plots demonstrated a significant 50% reduction in the 24 h mortality rate after CLP in the *P2RX₇^{-/-}* mice. A similar reduction was observed in mice pretreated with A438079 or anti-CXCL1 antibody (Figure 9F).

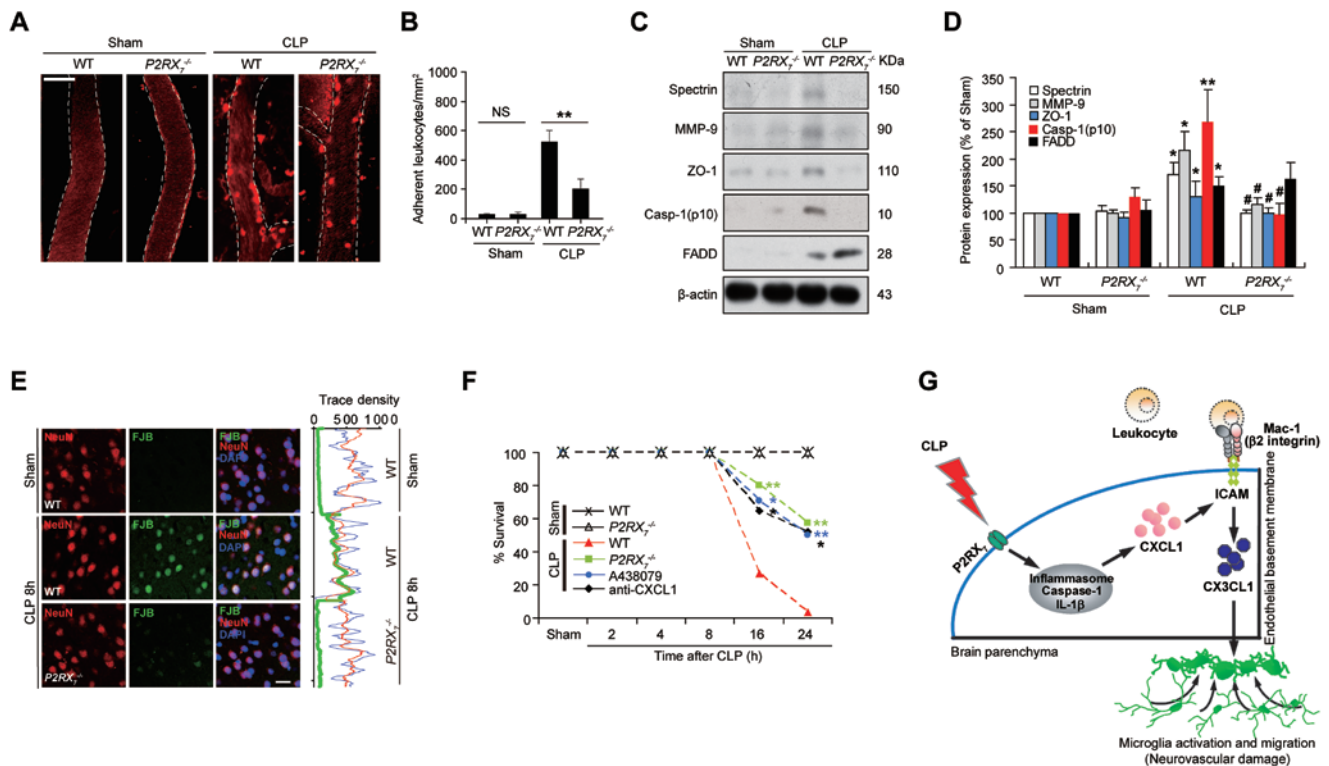


Figure 9 CLP-induced neurovascular injury is associated with endothelial P2RX₇ purinoreceptor pathway activation. **(A)** Representative images from intravital TPLSM analysis of adherent leukocytes in WT and P2RX₇^{-/-} mice 8 h after CLP. Scale bar, 30 μm. **(B)** Quantitative analysis of adherent leukocytes in WT and P2RX₇^{-/-} mice after CLP compared to sham-operated mice. Results are shown as means ± SEM (n = 4). **P < 0.01. NS, not significant. **(C)** Representative immunoblots showing spectrin, MMP-9, ZO-1, caspase-1(p10) and FADD expression in WT and P2RX₇^{-/-} mice 8 h after CLP. **(D)** Densitometry of western blots in **C** was normalized by the level of β-actin as an internal control. Data are expressed as densitometry ratio of sham (mean ± SEM, n = 4). *P < 0.05; **P < 0.01 versus WT (Sham); #P < 0.05 versus WT (CLP) mice. **(E)** The immunohistochemical staining for FJB (green) and NeuN (red) in WT and P2RX₇^{-/-} mice after CLP. FJB staining shows that the degree of neurodegeneration was decreased in P2RX₇^{-/-} mice 8 h after CLP. The graph on the right shows the relative intensity of the fluorescent signals. Scale bar, 20 μm. **(F)** Survival curve following CLP in P2RX₇^{-/-} mice, A438079-treated mice, CXCL1-neutralizing antibody-treated mice and WT littermates. Kaplan–Meier survival curves represented the percentage of surviving mice during the 24 h experimental protocol after CLP. n = 10–15, *P < 0.05; **P < 0.01 versus CLP (WT) mice. **(G)** Schematic illustration of endothelial P2RX₇-dependent mechanisms underlying leukocyte–endothelial cell adhesion and neurovascular damage under septic encephalopathy.

Discussion

Using dynamic *in vivo* imaging combined with genetic, pharmacological and molecular approaches, this study reveals the existence of a multistep process of directional cues that guide microglia toward the foci of damaged and inflamed brain vessels during sepsis. Specifically, this study suggests that the activation of endothelial P2RX₇ signaling generates an intravascular inflammatory microenvironment that leads to both leukocyte adhesion and microglial activation, thus providing a missing link between the two processes induced by sepsis. This study further shows that blockade of the P2RX₇ signaling

pathway using multiple approaches significantly protects animals from CLP-induced mortality, suggesting that the pathway may represent a novel therapeutic target for SE.

Intravital TPLSM provides micrometer spatial resolution deep within the cerebral tissue, permitting dynamic measurements of cell movement over long time intervals in living animals [34, 42]. Leukocyte–endothelial cell interaction is the rate-limiting step that controls the inflammatory progression of sepsis [43, 44]. Previously, *in vitro* biochemical analysis of leukocyte–endothelial cell adhesion [45] was unable to reflect the temporal and spatial changes underlying the pathological progression in the brains of septic mice. In this study, we used *in vivo*

TPLSM to record the dynamic pathogenesis of leukocyte adhesion in the brains of septic mice. Using this technique, this study provides the first *in vivo* evidence that sepsis increases leukocyte adhesion to the brain vasculature, and that this effect is associated with the marked activation of microglia and their migration towards the inflamed sites.

How do remotely activated endothelial cells orchestrate these dynamic changes in leukocyte adhesion and microglia activation? To address this question, we first examined the effect of CLP on endothelial chemokines and found that this procedure increased the mRNA expression of CXCL1. A role for CXCL1 in leukocyte adhesion was further confirmed by demonstrating that an anti-CXCL1 antibody significantly reduced the leukocyte adhesion induced by CLP. Our results are consistent with previous studies showing that the CXCL1 family cytokines promote leukocyte-endothelial cell adhesion in the brain during encephalomyelitis [30]. We further demonstrated that CXCL1 acted through the $\beta 2$ integrin/ICAM-1 pathway to increase not only leukocyte adhesion but also endothelial CX3CL1 expression. Our results from CD18 hypomorphic mutants also suggest that ICAM-1 expression is not sufficient to trigger CX3CL1 expression; rather, the binding of ICAM-1 to $\beta 2$ integrin is responsible for CX3CL1 expression. This is consistent with results indicating that microglial activation is highly correlated with the degree of leukocyte adhesion.

How does the sepsis induced by CLP result in the endothelial expression of CXCL1? To begin answering this question, we examined inflammatory-related molecular events with a focus on P2RX₇, because this protein has been implicated in inflammatory diseases of humans and animals [21, 46]. The response of P2RX₇ to a wide range of stimuli, its modulation of pro-inflammatory signaling and its provision of a transmembrane channel for large molecules, represent unique features found in members of the purinergic receptor family [22, 23]. In this study, the observed ATP-induced change in membrane conductance and its blockade by the P2RX₇ antagonist A438079 demonstrated that the P2RX₇ receptor is expressed on brain endothelial cells. We also observed that endothelial P2RX₇ activation occurred before microglial activation (Supplementary information, Figure S13). These results are consistent with previous reports that P2RX₇ is an ATP-gated purinoceptor channel that mediates inflammasome cascades [22, 23], and further suggest that brain endothelial P2RX₇ activation initiates sepsis-mediated neurovascular injury.

Blocking P2RX₇ signaling in P2RX₇-knockout mice reduced leukocyte adhesion, NLRP3/caspase-1/IL-1 β signaling, neurovascular damage and mortality following

CLP. A role for IL-1 β in this P2RX₇-mediated effect was suggested by the observation that anti-IL-1 β antibody treatment inhibited the upregulation of specific adhesion molecules on endothelial cells that are required for firm leukocyte adhesion. Pharmacological blockade or shRNA knockdown of P2RX₇ consistently reduced the brain microvasculature permeability of septic mice, indicating an important role for P2RX₇ in the initiation of leukocyte-endothelial cell adhesion. Based on these results, we conclude that brain endothelial P2RX₇ is likely to be a key and early requirement for inflammatory activation in SE and that its effect occurs at least in part via activation of the inflammasome and NLRP3/caspase-1/IL-1 β signaling to promote breakdown of the BBB and neurovascular injury during SE.

Additional evidence suggests that P2RX₇ activation promotes leukocyte adhesion by increasing the endothelial expression of CXCL1, which in turn engages the $\beta 2$ integrin/ICAM-1 pathway to promote endothelial activation and leukocyte adhesion. Consistent with this, P2RX₇ knockdown inhibited the expression of ICAM-1 in the brain microvascular endothelium, thereby decreasing the leukocyte-endothelial cell adhesion induced by sepsis. Indeed, CXCL1 possesses neutrophil chemoattractant activity that is regulated by interleukins to promote leukocyte adhesion to brain capillaries during toxin exposure [30, 47]. Our finding that a neutralizing CXCL1 antibody prevented the interaction between $\beta 2$ integrin and endothelial ICAM-1 after CLP revealed that CXCL1 is a prerequisite for the activation of the $\beta 2$ integrin/ICAM-1 pathway. Although inflammatory activation via chemotaxis can direct large numbers of microglia toward injured tissues [48], microglial localization is not dependent on CXCL1 receptors [49], implicating that other chemokines generated by activated endothelial cells might be involved. This study showed that in addition to CXCL1, CX3CL1 (also known as fractalkine) expression was significantly increased in brain microvessels during sepsis. CX3CL1 exerts a chemotactic effect on mononuclear, natural killer and endothelial cells [49, 50]. We showed that silencing the $\beta 2$ integrin/ICAM-1 pathway abrogated the CLP-induced increase in CX3CL1 expression, and administration of a CX3CL1-neutralizing antibody decreased microglial activation during sepsis. These results indicate that CX3CL1 expression is dependent on leukocyte adhesion to the endothelium and that CX3CR1-CX3CL1 signaling mediates chemotactic endothelial-cell-to-microglia communication. Evidence suggests that CX3CL1 can be anchored to CXCR1 receptors to recruit microglia, indicating another level of cooperation between CXCL1 and CX3CL1 in mediating microglial activation [49, 51]. As discussed earlier,

CXCL1 also regulates endothelial CX3CL1 expression via the β 2 integrin/ICAM-1 pathway. Taken together, our data demonstrate that endothelial P2RX₇ signaling generates an inflammatory microenvironment that triggers leukocyte adhesion to the inflamed vascular endothelium and subsequent activation of the microglia during SE.

In this study, we analyzed *in vivo* leukocyte-endothelial cell adhesion, microglial activation and neurovascular damage in septic mice using multiple approaches. The results reveal a complex sepsis-induced cerebral inflammatory cascade leading to neurovascular damage that is initiated by endothelial P2RX₇ signaling (Figure 9G). Recently, an activating single-nucleotide polymorphism in P2RX₇ was shown to increase the risk of death in patients with severe sepsis [52]. Presently, only supportive therapy is available for the treatment of SE, which is associated with high mortality [53-55]. A clear implication of our results in this mouse model is that blockade of the P2RX₇ pathway may be useful for the prevention of neurovascular damage during SE, potentially providing the first rational and targeted therapy for this devastating condition.

Materials and Methods

Animals

CD18 hypomorphic mutant mice (B6.129S7-Itgb2^{tm1Bay}/J mice; Jackson Laboratories) [56], heterozygous *Cx3cr1*^{GFP/+} mice (B6.129P-Cx3cr1^{tm1Lit}/J mice; Jackson Laboratories) [57], and P2RX₇ KO mice (B6.129P2-P2rx7^{tm1Gab}/J; Jackson Laboratories) [22] were used in this study. Wild-type C57BL/6J mice or littermate mice were used as controls. Mice (2-3 months old, 22-25 g) were group housed on a 12-h light/dark cycle at a constant temperature of 22 ± 1 °C with 40-60% humidity. All animal studies were approved by the Committees for Animal Experiments of Zhejiang University in China and conformed to NIH guidelines (Guide for the Care and Use of Laboratory Animals. NIH publication no. 85-23, revised 1996).

CLP model and drug treatment

Sepsis was induced by CLP [58] and compared to sham-operated controls. Briefly, mice were anesthetized with chloral hydrate (400 mg/kg body weight) and, through a midline celiotomy, the cecum was ligated distal to the ileocecal valve and punctured with an 18-gauge needle to allow feces to enter the peritoneal cavity. A control group was sham-operated. The mice were intravenously administered with either saline or other agents, including A438079 (80 mg/kg, P2RX₇ antagonist, Tocris Bioscience, Bristol, UK), anti-IL-1 β mAb (100 μ g/mouse, AB-401-NA, R&D Systems, Minneapolis, MN, USA) or anti-CXCL1 mAb (50 μ g/mouse, AB-401-NA, R&D Systems), anti-CX3CL1 mAb (15 μ g/mouse, AB-401-NA, R&D Systems), anti-CCL2/JE/MCP-1 mAb (10 mg/kg, AF-479-NA, R&D Systems) and anti-CXCL7/Thymus Chemokine-1 mAb (50 mg/kg, AF793, R&D Systems), at 1 h after CLP surgery. Normal Goat IgG (R&D Systems), Rat IgG2A isotype Control (R&D Systems) were used as isotype control and administered us-

ing the same dosing schedule. For neutrophil depletion, mice were treated with intraperitoneal injection of 250 μ g anti-granulocyte receptor-1 (Gr-1) mAb RB6-8C5 (BioXCell, West Lebanon, NH, USA) or an isotype control (BioXCell) 24 h prior to CLP surgery. Assessments were made by two independent observers who were blind to genotype and treatment status.

Preparation of mice for *in vivo* imaging by intravital TPLSM

The cerebral blood vessels of anesthetized adult male mice were imaged through a craniotomy window [59] centered at stereotaxic coordinates 2.5 mm caudal to bregma and 2.5 mm lateral to the midline to study *in vivo* leukocyte adhesion. Following removal of the dura, a 10 mm diameter metal frame with a removable GOMN glass lid were glued to the skull. The space between the exposed brain surface and the glass cover was filled with 1.5% (w/v) low-melting-point agarose in artificial cerebrospinal fluid.

TPLSM imaging and analysis

Stacked or single focal plane two-photon images were obtained with an upright Olympus laser scanning confocal microscope (BX61W1-FV1000, Olympus, Tokyo, Japan) with an excitation source of a Spectra-Physics MaiTai HP DeepSee femtosecond Ti:Sa laser. For studies of leukocyte adhesion, leukocytes were stained *in vivo* with an intravenous bolus injection of 50 μ l of a 0.01% solution of rhodamine 6G (Sigma-aldrich, St Louis, MO, USA) [60]. For microglia study, we used GFP-positive microglia transgenic mice *Cx3cr1*^{GFP/+}. A long-working distance (2 mm) water-immersion objective (25 \times , NA = 1.05) was adopted for *in vivo* bioimaging. The images were taken at 12-bit depth with resolution of 1024 \times 1024 pixels.

Adherent leukocytes were quantified as the number of leukocytes that were sufficiently firmly attached to the endothelium to remain in place for over 1 min. Cortical brain vessels 20-40 μ m in diameter and 100-150 μ m in depth below the cortical surface were selected for two-photon imaging. Z-stack images of 50- μ m thickness tissue at 1- μ m steps were collected and three-dimensional pictures were constructed by Imaris Imaging Software (Bitplane) to calculate the number of leukocytes adherent to 100 μ m of vessel segment.

The vessel imaging and analysis were performed as previously reported [61]. Briefly, an Olympus Fluoview1000 two-photon microscope (BX61W1-FV1000, Olympus) with an excitation source of a Spectra-Physics MaiTai HP DeepSee femtosecond Ti:Sa laser was used. A long-working distance (2 mm) water-immersion objective (25 \times , NA = 1.05) was used to measure leukocyte movement in mouse brain vessels. The images were taken at 12-bit depth with resolution of 1024 \times 1024 pixels. Leukocyte rolling velocity was measured for neutrophils entering the field of view at each time point by transillumination intravital microscopy. *In vivo* vessel diameters were measured manually using Image J (NIH, Bethesda, MD, USA).

Lentiviral transduction of P2RX₇ shRNA

P2RX₇ short-hairpin RNA (shRNA) expression plasmids were constructed from two complementary P2RX₇ DNA oligonucleotides that were synthesized, annealed and inserted into a pMagic 4.1 plasmid as previously described [22]. Reduced P2RX₇ expression in mouse brain was achieved through intracerebroventricular

injection (anteroposterior, AP -0.5 mm; mediolateral, ML -1.0 mm; dorsoventral, DV -3.0 mm) of $5 \mu\text{l}$ LV-*P2RX₇* shRNA (1×10^9 transducing units (TU)/ml). The effect of *P2RX₇* shRNA transfection on CLP-induced leukocyte-endothelial cell adhesion was analyzed 2 weeks after lentiviral transduction.

Electrophysiology

Electrophysiological patch clamp recordings were performed on HBMEC as previously described [39]. HBMEC cell line used in this study was obtained from ScienCell Research Laboratories (San Diego, CA, USA). To measure activation of nonselective cation channel currents by ATP, the holding potential was set to 0 mV to eliminate any possible contributions by voltage-dependent Ca^{2+} channels. Whole-cell currents were recorded for 400 ms using a series of voltage pulses from -70 to $+100$ mV (10 mV increments) and were normalized to cell membrane capacitance to calculate current density (pA/pF).

Cell preparation and flow cytometry analyses

Peripheral blood was collected from mice before decapitation and used for flow cytometry as described previously [62, 63]. Mouse brain endothelial cells were isolated as described [64]. The mouse brain cortex was removed and digested with freshly prepared Dulbecco's modified Eagle's medium (DMEM) containing 5 mM Ca^{2+} , 10 mM HEPES, 400 U/ml collagenase (Sigma), and 10 mg/ml DNase I (Roche). After continuous stirring for 1.25 h at 37°C , the solution was centrifuged at $1\,000\times g$ for 5 min; then, the pellet was resuspended in DMEM solution containing 20% w/v bovine serum albumin (BSA, Roche) and centrifuged at $1\,000\times g$ for 20 min. The resulting pellets were further digested with 1 mg/ml collagenase and Dnase I in DMEM for 40 min at 37°C . A concentration of 5 mM EDTA was added to the vessel solution and centrifuged, and cellular populations were filtered through a $100 \mu\text{m}$ strainer (BD Falcon, San Jose, CA, USA). The enriched endothelial cells at the bottom were collected for use in flow cytometry, western blotting and real-time quantitative RT-PCR. For flow cytometry [65], cells were resuspended in buffer (1% BSA in PBS) and incubated for 30 min in the dark at 4°C with antibodies (eBioscience) initially at $1:500$ to detect specific cell-surface markers, including: PE-CD18(M18/2); PE-CD11a(M17/4); PE-CD11b(M1/70); APC-Ly6G (RB6-8c5); PE-CD54 (KAT-1); FITC-CD106 (429) and APC-CD31 (390). Isotype-matched control antibodies (eBioscience) were used as negative controls at the same concentration as the corresponding antibody. In each measurement, $10\,000$ events were analyzed. Flow cytometry data were analyzed using FlowJo 7.6 software (TreeStar).

Western blotting

The total brain [66] and microvessel protein extracts [64] from mouse homogenized cerebral cortex were prepared for western blotting. Samples containing equal amounts of protein were loaded onto 10% - 13.5% acrylamide denaturing gels (SDS-PAGE) for protein separation. Proteins were then transferred to an Immobilon polyvinylidene difluoride membrane for 1 h at 50 V. Then membrane were blocked in 20 mM Tris-HCl (pH 7.4), 150 mM NaCl and 0.1% Tween 20 (TBS-T) containing 5% fat-free milk powder for 1 h and probed overnight at 4°C with antibodies against zonula occludens-1 (ZO-1) (Invitrogen, Carlsbad, CA, USA), spectrin and MMP-9 (Millipore, Billerica, MA, USA), *P2RX₇* (Abcam,

Cambridge, MA, USA), FADD (Epitomics, CA, USA) and β -actin (Sigma Chemical, St. Louis, MO, USA). Caspase-1 (sc-56036, Santa Cruz Biotechnology, Santa Cruz, CA, USA) was used to detect ProCaspase-1, Caspase-1 (sc-514, Santa Cruz Biotechnology) was used to detect Caspase-1(p10), IL- 1β (sc-7884, Santa Cruz Biotechnology) was used to detect ProIL- 1β , and IL- 1β (D4T2D, Cell Signaling Technology, Danvers, MA, USA) was used to detect IL- 1β (p17). Bands were visualized by enhanced chemiluminescence (Amersham Life Science, Buckinghamshire, UK). Immunoreactive band intensities were analyzed by Image J software (NIH). The band was normalized against the corresponding β -actin band used as loading control.

RNA isolation and real-time quantitative RT-PCR

Mouse brain endothelial cells were isolated as described above [63], snap frozen in liquid nitrogen, and stored at -80°C until use. Samples were homogenized and total RNA was isolated using RNAiso Plus (Takara, Shiga, Japan). RNA samples with $260/280$ ratio from 1.9 to 2.1 (Bio-Rad SmartSpec 3000) were used for further analysis. First strand cDNA was synthesized by reverse transcribing 500 ng of total RNA with the PrimeScript RT reagent Kit Perfect Real Time (Takara) in a $20 \mu\text{l}$ reaction using random primers according to the manufacturer's instructions. Chemokine mRNA expression was determined by real-time quantitative RT-PCR. qRT-PCR was performed in 96 -well plates with a Mastercycler ep realplex (Eppendorf, Hamburger, Germany) using SYBR Premix Ex Taq (Takara). PCR conditions were as follows: 95°C for 2 min, 40 cycles of each 95°C for 15 s, 55°C for 15 s and 68°C for 25 s. Melting curve analysis was performed with the default settings on the instrument from 50°C to 85°C . The Ct values were automatically calculated using commercial software with the Mastercycler ep realplex. The details of primer sequences are provided in Supplementary information, Table S1.

Immunohistochemical labeling, image acquisition and analysis

Animals were anesthetized and transcardially perfusion-fixed with 4% paraformaldehyde in phosphate-buffered saline (PBS) as described previously [66]. In brief, whole brains were removed immediately and post-fixed overnight at 4°C in the same fixative. For immunolabeling, coronal brain sections anterior or posterior to the bregma ($35 \mu\text{m}$ in thickness) were prepared using a micro-slicer system (Vibratome, St. Louis, MO, USA). Brain sections (post bregma begins ~ 2.18 mm) were incubated at room temperature with 0.01% Triton, X-100 in PBS for 30 min followed by incubation in 3% BSA in PBS for 1 h. Sections were incubated with antibodies to *P2RX₇* (Abcam), CD31 (Santa Cruz Biotechnology), ICAM-1 (Santa Cruz Biotechnology), Iba1 (rabbit polyclonal; WAKO, Japan), CX3CL1 (Abcam) and CXCL1 (R&D Systems) overnight at 4°C , followed by exposure to fluorescent secondary antibodies according to a standard protocol from PerkinElmer Life Sciences (Boston, MA, USA). Immunofluorescent images of brain cortex were taken with a confocal laser scanning microscope (Zeiss LSM 510 META, Carl Zeiss, Germany), and fluorescence density was analyzed using Image J software (NIH). Morphological parameters of microglia cells were defined to characterize the activation of microglia, including soma size and eccentricity (the ratio of the major axis to the minor axis) [29]. All parameters were calculated by using the software package MATLAB R2011b

(Mathworks, USA) and Image J software.

BV-2 murine microglial cell culture and migration assay

Migration of BV-2 murine microglial cells was assessed with a transwell migration chamber. BV2 cell line was obtained from the American Type Culture Collection (Manassas, VA, USA). Migration was induced by recombinant CXCL1 (100 ng/ml, R&D systems, Catalog #: 275-GR-010/CF) or recombinant CX3CL1 (10 nM, Sino Biological, Catalog #: 10636-H08H) with or without LPS from *Escherichia coli* 055:B5 (100 ng/ml, Sigma-Aldrich) in the lower chamber. The number of cells in each well was normalized to the average number of cells in the control condition (100%) [22].

Ethidium uptake assay

Measurements of Et⁺ influx and ethidium uptake assay were performed as previously reported [39]. Briefly, HBMEC were plated for 4 h in complete medium in a gelatin-coated 96-well black plate at a seeding density of 1.5×10^6 /ml. Complete medium was removed and cells were incubated in PBS containing 25 μ M Ethidium bromide (Sigma-Aldrich) at 37 °C. Before Fluorescent measurements, ATP and P2RX₇ antagonist (A438079, 10 μ M) were added into PBS of 96-well plates at 37 °C. Fluorescent measurements were performed using a DTX 880 multimode detector (Beckman Coulter, Brea, CA, USA) with excitation wavelength of 540 nm and emission wavelength of 590 nm. One mM ATP treatment in the absence or presence of P2RX₇ antagonist was compared with control group.

Chemokine assays

Whole-blood samples were harvested and serum samples were isolated. CXCL1 and CX3CL1 levels in serum from sham and CLP animals were measured using the mouse ELISA kit (Elabscience Biotechnology), according to the manufacturer's instructions.

FJB staining

Brain sections (post bregma begins ~2.18 mm) were immersed in a 0.06% KMnO₄ for 10 min, rinsed in distilled water for 1 min and transferred to FJB staining solution (Millipore; 0.001%) for 10 min and rinsed [22].

Statistics

The data for two-group comparisons were analyzed with a two-tailed unpaired *t*-test (parametric data) and for multi-group comparisons, results were analyzed using one-way analysis of variance followed by a *post hoc* Tukey's test or Dunnett's comparison to control. Data are expressed as mean \pm SEM with significance taken by *P* < 0.05.

Acknowledgments

This work was supported in part by the National Natural Science Foundation of China (81120108023, 81302748 and 81300991), the Zhejiang Provincial Natural Science Foundation of China (LQ13H310001), and NIH (HL68686, DK49870 and DK36079).

References

- Brown KA, Brain SD, Pearson JD *et al.* Neutrophils in development of multiple organ failure in sepsis. *Lancet* 2006; **368**:157-169.
- Rittirsch D, Flierl MA, Ward PA. Harmful molecular mechanisms in sepsis. *Nat Rev Immunol* 2008; **8**:776-787.
- Mao K, Chen S, Chen M, *et al.* Nitric oxide suppresses NLRP3 inflammasome activation and protects against LPS-induced septic shock. *Cell Res* 2013; **23**:201-212.
- Pytel P, Alexander JJ. Pathogenesis of septic encephalopathy. *Curr Opin Neurol* 2009; **22**:283-287.
- Iwashyna TJ, Ely EW, Smith DM, Langa KM. Long-term cognitive impairment and functional disability among survivors of severe sepsis. *JAMA* 2010; **304**:1787-1794.
- Semmler A, Widmann CN, Okulla T, *et al.* Persistent cognitive impairment, hippocampal atrophy and EEG changes in sepsis survivors. *J Neurol Neurosurg Psychiatry* 2013; **84**:62-69.
- Taccone FS, Su F, De Deyne C, *et al.* Sepsis is associated with altered cerebral microcirculation and tissue hypoxia in experimental peritonitis. *Crit Care Med* 2014; **42**:e114-122.
- Koedel U, Rupprecht T, Angele B, *et al.* MyD88 is required for mounting a robust host immune response to *Streptococcus pneumoniae* in the CNS. *Brain* 2004; **127**:1437-1445.
- Opal SM, Laterre PF, Francois B, *et al.* Effect of eritoran, an antagonist of MD2-TLR4, on mortality in patients with severe sepsis: the ACCESS randomized trial. *JAMA* 2013; **309**:1154-1162.
- David S, Kumpers P, van Slyke P, Parikh SM. Mending leaky blood vessels: the angiopoietin-Tie2 pathway in sepsis. *J Pharmacol Exp Ther* 2013; **345**:2-6.
- Ince C, Sinaasappel M. Microcirculatory oxygenation and shunting in sepsis and shock. *Crit Care Med* 1999; **27**:1369-1377.
- Hernandez G, Bruhn A, Ince C. Microcirculation in sepsis: new perspectives. *Curr Vasc Pharmacol* 2013; **11**:161-169.
- Osuchowski MF, Craciun F, Weixelbaumer KM, Duffy ER, Remick DG. Sepsis chronically in MARS: systemic cytokine responses are always mixed regardless of the outcome, magnitude, or phase of sepsis. *J Immunol* 2012; **189**:4648-4656.
- Osuchowski MF, Welch K, Yang H, Siddiqui J, Remick DG. Chronic sepsis mortality characterized by an individualized inflammatory response. *J Immunol* 2007; **179**:623-630.
- Khamisi R. Execution of sepsis trials needs an overhaul, experts say. *Nat Med* 2012; **18**:998-999.
- Comim CM, Vilela MC, Constantino LS, *et al.* Traffic of leukocytes and cytokine up-regulation in the central nervous system in sepsis. *Intensive Care Med* 2011; **37**:711-718.
- Goldmann T, Tay TL, Prinz M. Love and death: microglia, NLRP3 and the Alzheimer's brain. *Cell Res* 2013; **23**:595-596.
- Dou Y, Wu HJ, Li HQ, *et al.* Microglial migration mediated by ATP-induced ATP release from lysosomes. *Cell Res* 2012; **22**:1022-1033.
- Cunningham C. Microglia and neurodegeneration: the role of systemic inflammation. *Glia* 2013; **61**:71-90.
- van den Boogaard M, Ramakers BP, van Alfen N, *et al.* Endotoxemia-induced inflammation and the effect on the human

- brain. *Crit Care* 2010; **14**:R81.
- 21 Chiao CW, Da SJ, Giachini FR, et al. P2X7 receptor activation contributes to an initial upstream mechanism of lipopolysaccharide-induced vascular dysfunction. *Clin Sci* 2013; **125**:131-141.
- 22 Lu YM, Tao RR, Huang JY, et al. P2X7 signaling promotes microsphere embolism-triggered microglia activation by maintaining elevation of Fas ligand. *J Neuroinflammation* 2012; **9**:172.
- 23 Choi HB, Ryu JK, Kim SU, McLarnon JG. Modulation of the purinergic P2X7 receptor attenuates lipopolysaccharide-mediated microglial activation and neuronal damage in inflamed brain. *J Neurosci* 2007; **27**:4957-4968.
- 24 Babelova A, Moreth K, Tsalastra-Greul W, et al. Biglycan, a danger signal that activates the NLRP3 inflammasome via toll-like and P2X receptors. *J Biol Chem* 2009; **284**:24035-24048.
- 25 Zauner C, Gendo A, Kramer L, et al. Impaired subcortical and cortical sensory evoked potential pathways in septic patients. *Crit Care Med* 2002; **30**:1136-1139.
- 26 Choi EY, Chavakis E, Czabanka MA, et al. Del-1, an endogenous leukocyte-endothelial adhesion inhibitor, limits inflammatory cell recruitment. *Science* 2008; **322**:1101-1104.
- 27 Cardona AE, Pioro EP, Sasse ME, et al. Control of microglial neurotoxicity by the fractalkine receptor. *Nat Neurosci* 2006; **9**:917-924.
- 28 Marker DF, Tremblay ME, Lu SM, Majewska AK, Gelbard HA. A thin-skull window technique for chronic two-photon *in vivo* imaging of murine microglia in models of neuroinflammation. *J Vis Exp* 2010; **43**:pii: 2059.
- 29 Kozlowski C, Weimer RM. An automated method to quantify microglia morphology and application to monitor activation state longitudinally *in vivo*. *PLoS One* 2012; **7**:e31814.
- 30 Roy M, Richard JF, Dumas A, Vallieres L. CXCL1 can be regulated by IL-6 and promotes granulocyte adhesion to brain capillaries during bacterial toxin exposure and encephalomyelitis. *J Neuroinflammation* 2012; **9**:18.
- 31 Pachot A, Cazalis MA, Venet F, et al. Decreased expression of the fractalkine receptor CX3CR1 on circulating monocytes as new feature of sepsis-induced immunosuppression. *J Immunol* 2008; **180**:6421-6429.
- 32 Xu J, Gao XP, Ramchandran R, et al. Nonmuscle myosin light-chain kinase mediates neutrophil transmigration in sepsis-induced lung inflammation by activating beta2 integrins. *Nat Immunol* 2008; **9**:880-886.
- 33 Tang Z, Gan Y, Liu Q et al. CX3CR1 deficiency suppresses activation and neurotoxicity of microglia/macrophage in experimental ischemic stroke. *J Neuroinflammation* 2014; **11**:26.
- 34 Liang KJ, Lee JE, Wang YD, et al. Regulation of dynamic behavior of retinal microglia by CX3CR1 signaling. *Invest Ophthalmol Vis Sci* 2009; **50**:4444-4451.
- 35 Rao P, Hayden MS, Long M, et al. IkappaBbeta acts to inhibit and activate gene expression during the inflammatory response. *Nature* 2010; **466**:1115-1119.
- 36 Tannahill GM, Curtis AM, Adamik J, et al. Succinate is an inflammatory signal that induces IL-1beta through HIF-1alpha. *Nature* 2013; **496**:238-242.
- 37 Clark AK, Staniland AA, Marchand F, et al. P2X7-dependent release of interleukin-1beta and nociception in the spinal cord following lipopolysaccharide. *J Neurosci* 2010; **30**:573-582.
- 38 van Buul JD, van Rijssel J, van Alphen FP, et al. ICAM-1 clustering on endothelial cells recruits VCAM-1. *J Biomed Biotechnol* 2010; **2010**:120328.
- 39 Thompson BA, Storm MP, Hewinson J, et al. A novel role for P2X7 receptor signalling in the survival of mouse embryonic stem cells. *Cell Signal* 2012; **24**:770-778.
- 40 Norenberg W, Hempel C, Urban N, et al. Clemastine potentiates the human P2X7 receptor by sensitizing it to lower ATP concentrations. *J Biol Chem* 2011; **286**:11067-11081.
- 41 Sugiyama T, Kawamura H, Yamanishi S, et al. Regulation of P2X7-induced pore formation and cell death in pericyte-containing retinal microvessels. *Am J Physiol Cell Physiol* 2005; **288**:C568-C576.
- 42 Blinder P, Tsai PS, Kaufhold JP, et al. The cortical angiome: an interconnected vascular network with noncolumnar patterns of blood flow. *Nat Neurosci* 2013; **16**:889-897.
- 43 Zonneveld R, Martinelli R, Shapiro NI, Kuijpers TW, Plötz FB, Carman CV. Soluble adhesion molecules as markers for sepsis and the potential pathophysiological discrepancy in neonates, children and adults. *Crit Care* 2014; **18**:204.
- 44 Schmidt EP, Yang Y, Janssen WJ, et al. The pulmonary endothelial glycocalyx regulates neutrophil adhesion and lung injury during experimental sepsis. *Nat Med* 2012; **18**:1217-1223.
- 45 Wang R, Wang Y, Liu N, et al. FBW7 regulates endothelial functions by targeting KLF2 for ubiquitination and degradation. *Cell Res* 2013; **23**:803-819.
- 46 Chen L, Brosnan CF. Regulation of immune response by P2X7 receptor. *Crit Rev Immunol* 2006; **26**:499-513.
- 47 Rabers NA, Nottet HS. Role of the pro-inflammatory cytokines TNF-alpha and IL-1beta in HIV-associated dementia. *Eur J Clin Invest* 2006; **36**:447-458.
- 48 Johnson EA, Dao TL, Guignet MA, et al. Increased expression of the chemokines CXCL1 and MIP-1alpha by resident brain cells precedes neutrophil infiltration in the brain following prolonged soman-induced status epilepticus in rats. *J Neuroinflammation* 2011; **8**:41.
- 49 Lucas AD, Bursill C, Guzik TJ, et al. Smooth muscle cells in human atherosclerotic plaques express the fractalkine receptor CX3CR1 and undergo chemotaxis to the CX3C chemokine fractalkine (CX3CL1). *Circulation* 2003; **108**:2498-2504.
- 50 Imaizumi T, Yoshida H, Satoh K. Regulation of CX3CL1/fractalkine expression in endothelial cells. *J Atheroscler Thromb* 2004; **11**:15-21.
- 51 Johnson LA, Jackson DG. The chemokine CX3CL1 promotes trafficking of dendritic cells through inflamed lymphatics. *J Cell Sci* 2013; **126**:5259-5270.
- 52 Geistlinger J, Du W, Groll J, et al. P2RX7 genotype association in severe sepsis identified by a novel Multi-Individual Array for rapid screening and replication of risk SNPs. *Clin Chim Acta* 2012; **413**:39-47.
- 53 Williams SC. After Xigris, researchers look to new targets to combat sepsis. *Nat Med* 2012; **18**:1001.
- 54 Yealy DM, Kellum JA, Huang DT, et al. A randomized trial of protocol-based care for early septic shock. *N Engl J Med* 2014; **370**:1683-1693.
- 55 Marzocchetti A, Tompkins T, Clifford DB, et al. Determinants of survival in progressive multifocal leukoencephalopathy.

- Neurology* 2009; **73**:1551-1558.
- 56 Gorina R, Lyck R, Vestweber D, Engelhardt B. β 2 integrin-mediated crawling on endothelial ICAM-1 and ICAM-2 is a prerequisite for transcellular neutrophil diapedesis across the inflamed blood-brain barrier. *J Immunol* 2014; **192**:324-337.
- 57 Ponomarev ED, Veremeyko T, Barteneva N, Krichevsky AM, Weiner HL. MicroRNA-124 promotes microglia quiescence and suppresses EAE by deactivating macrophages via the C/EBP- α -PU.1 pathway. *Nat Med* 2011; **17**:64-70.
- 58 Rittirsch D, Huber-Lang MS, Flierl MA, Ward PA. Immunodesign of experimental sepsis by cecal ligation and puncture. *Nat Protoc* 2009; **4**:31-36.
- 59 Shih AY, Driscoll JD, Drew PJ, *et al.* Two-photon microscopy as a tool to study blood flow and neurovascular coupling in the rodent brain. *J Cereb Blood Flow Metab* 2012; **32**:1277-1309.
- 60 Ramirez SH, Haskó J, Skuba A, *et al.* Activation of cannabinoid receptor 2 attenuates leukocyte-endothelial cell interactions and blood-brain barrier dysfunction under inflammatory conditions. *J Neurosci* 2012; **32**:4004-4016.
- 61 Huang JY, Li LT, Wang H, *et al.* *In vivo* two-photon fluorescence microscopy reveals disturbed cerebral capillary blood flow and increased susceptibility to ischemic insults in diabetic mice. *CNS Neurosci Ther* 2014; **20**:816-822.
- 62 Ribes S, Regen T, Meister T, *et al.* Resistance of the brain to *Escherichia coli* K1 infection depends on MyD88 signaling and the contribution of neutrophils and monocytes. *Infect Immun* 2013; **81**:1810-1819.
- 63 Ferri LE, Chia S, Benay C, Giannias B, Christou NV. L-selectin shedding in sepsis limits leukocyte mediated microvascular injury at remote sites. *Surgery* 2009; **145**:384-391.
- 64 Calabria AR, Weidenfeller C, Jones AR, de Vries HE, Shusta EV. Puromycin-purified rat brain microvascular endothelial cell cultures exhibit improved barrier properties in response to glucocorticoid induction. *J Neurochem* 2006; **97**:922-933.
- 65 Wu Z, Hofman FM, Zlokovic BV. A simple method for isolation and characterization of mouse brain microvascular endothelial cells. *J Neurosci Methods* 2003; **130**:53-63.
- 66 Han F, Tao RR, Zhang GS, *et al.* Melatonin ameliorates ischemic-like injury-evoked nitrosative stress: Involvement of HtrA2/PED pathways in endothelial cells. *J Pineal Res* 2011; **50**:281-291.

(Supplementary information is linked to the online version of the paper on the *Cell Research* website.)



This work is licensed under the Creative Commons Attribution-NonCommercial-No Derivative Works 3.0 Unported License. To view a copy of this license, visit <http://creativecommons.org/licenses/by-nc-nd/3.0>